Fuel 115 (2014) 190–202

Contents lists available at SciVerse ScienceDirect

Fuel

journal homepage: www.elsevier.com/locate/fuel

Characterization of polar compounds in a true boiling point distillation system using electrospray ionization FT-ICR mass spectrometry

Guilherme P. Dalmaschio [a], Majorie M. Malacarne [a], Vinicius M.D.L. de Almeida [a], Thieres M.C. Pereira [a], Alexandre O. Gomes [b], Eustaquio V.R. de Castro [a], Sandro J. Greco [a], Boniek G. Vaz [c,*], Wanderson Romão [a,d,*]

[a] Department of Chemistry, Federal University of Espírito Santo, 29075-910 Vitória, ES, Brazil
[b] Petróleo Brasileiro S/A – PETROBRAS, CENPES, Rio de Janeiro, RJ, Brazil
[c] Chemistry Institute, Federal University of Goiás, 74001-970 Goiânia, GO, Brazil
[d] Federal Institute of Education, Science and Technology of Espírito Santo, 29106-010 Vila Velha, ES, Brazil

HIGHLIGHTS

- We describe the typification of polar compounds of twelve cuts obtained from a true boiling point system.
- We examine changes in the cuts composition by ESI(−) FT-ICR MS analysis.
- A correlation between the composition and TAN, total sulfur and the corrosion process was performed.
- The structures of some naphthenic acids, phenols and pyridines were confirmed using ESI(±)-MS/MS.

ARTICLE INFO

Article history:
Received 4 May 2013
Received in revised form 28 June 2013
Accepted 1 July 2013
Available online 14 July 2013

Keywords:
Petroleomics
Distillation system
Mass spectrometry
FT-ICR MS
Methylation reactions

ABSTRACT

In this work, electrospray ionization Fourier transform ion cyclotron resonance mass spectrometry (ESI(±)-FT-ICR MS) was applied in the chemical characterization of polar compounds. These compounds were identified as the oxygen-containing compound classes (naphthenic acids, O2 class, and phenols, O1 class), the sulfur-containing compound classes (mainly sulfides, S1 class), and the basic and non-basic nitrogen-containing compound classes (carbazoles and pyridines, N class). For access the sulfur-containing compounds were employed the methylation reactions. As the increasing of distillation cut temperature, the amount of O2 compounds increased (from 9 for cut 2 to 66 for cut 12), and the average molecular weight distribution, M_w, shifted to higher m/z values (M_w = 169 → 321 Da). These results were consistent with the increase of TAN with the boiling point. Plots of the DBE versus the carbon number for the O2 class of heavy distillation cuts (cuts 4–12) suggested a maximum abundance of the carbon numbers located at C_{12}–C_{18} with a constant DBE of 3. For the nitrogen-containing compounds, 100 compounds were detected with m/z ranging from 160 to 414. Similar to O2 class, the amount of nitrogen species increased, and the M_w shifted for high values in function of distillation cut temperature: 6 species and M_w = 206 Da for cut 3; and 64 species and M_w = 340 Da for cut 12. The structures and the connectivity of naphthenic acids, phenols and pyridines were confirmed using ESI(±)-MS/MS. The most abundant sulfur compounds in heavy distillation cuts presented a carbon number of C_{23} (for cut 11) and C_{25} (for cut 12) with constant DBE of 3. Results of ESI(±)-FT-ICR MS contributed to the understanding of the chemical composition of Brazilian crude oil and the establishment of a correlation with the corrosion process.

1. Introduction

The chemical composition of crude oil consists predominantly of hydrocarbon compounds such as naphthenes, paraffins, and aromatic hydrocarbons (~90%). The remainder (~10%) consists of polar compounds containing N, O, and S heteroatoms and metal atoms (only vanadium and nickel exist at concentrations >1 ppm) [1]. Despite the small percentage of polar compounds, approximately 20,000 polar organic compounds with different elemental compositions ($C_cH_hN_nO_oS_s$) have been found in crude oil [2]. These polar compounds sometimes cause problems during the production, refining and storage of petroleum. These problems include corrosion, the formation of emulsions, the poisoning of catalysts,

* Corresponding authors. Tel.: +55 62 3521 1016xR261 (Boniek G. Vaz), tel.: +55 27 3149 0833 (W. Romão).
E-mail addresses: boniek@quimica.ufg.br (B.G. Vaz), wandersonromao@gmail.com (W. Romão).

0016-2361/$ - see front matter © 2013 Elsevier Ltd. All rights reserved.
http://dx.doi.org/10.1016/j.fuel.2013.07.008

coke formation, the development of poisonous and carcinogenic characteristics, and contamination. Oil consumption is continuously growing, which creates the demand to use the limited oil reservoirs and the heavier fractions more efficiently. Therefore, it is extremely important to know the composition of crude oils from different origins to optimize the refining processes.

Among the polar components of petroleum that contain heteroatoms, naphthenic acids and phenols are the two most common oxygen-containing compound classes in crude oil. There are other minor acidic classes, such as aromatic, olefinic, hydroxyl, and dibasic acids [3]. Naphthenic acids are defined as carboxylic acids that include one or more saturated ring structures, with five- and six-membered rings being the most common. In addition to the ring-containing acids, linear carboxylic acids are often included in the naphthenic acid class [4]. Naphthenic acids are known to be a significant source of corrosion in oil-refining equipment [5]. Corrosion is associated with the total acid number (TAN), which is defined as the mass of potassium hydroxide (KOH) in milligrams required to neutralize 1 g of crude oil. However, it has been argued that there is no clear correlation between the TAN and the level of corrosion [6,7].

Recently, there has been growing interest in the chemical characterization of naphthenic acids and sulfur species from crude oils and its distillation cuts because of the problems that these components have caused for the oil refinery business [8]. These compounds induce corrosion in regions of the refineries that operate at temperatures above 100.0 °C. Sulfur compounds are the most notorious and undesirable petroleum contaminants, and a large portion of these compounds can be transferred to diesel oil during refining process. In general, sulfur appears in the form of hydrogen sulfide, organic sulfides and disulfides, benzothiophene, dibenzothiophene, and their alkylated derivatives [9]. Upon diesel combustion, sulfur compounds are converted to sulfur oxides (SOx), which contribute to acid rain and environmental pollution [10]. Although environmental regulation has been applied in many countries to reduce the sulfur levels in diesel and other fuels, sulfur removal still represents a major operational and economic challenge for the petroleum refining industry.

Other well-known polar components in petroleum are the neutral and basic nitrogen species. The non-basic nitrogen compounds usually include pyrrole, indole, carbazole, and their alkylated derivatives, and these compounds correspond to less than 30% of all organic nitrogen compounds [11]. The basic nitrogen compounds include amines, aniline, pyridine, quinoline, benzoquinoline, and their alkylated and hydrogenated derivatives. It is well known that the presence of the nitrogen compounds in liquid hydrocarbon streams, even at very low concentration, strongly deactivates the catalysts that are used in the fuel-refining processes, such as hydrodesulfurization (HDS), hydrodearomatization (HDA), hydrocracking, and reforming [12]. Therefore, the identification and quantification of the various nitrogen compounds and the clarification of their distribution in different liquid hydrocarbon streams are essential to develop either a novel process [13], more efficient catalysts or more efficient adsorbents for the denitrogenation of various liquid hydrocarbon streams and to understand the mechanism in ultradeep HDS, hydrodenitrogenation (HDN), adsorptive denitrogenation (ADN), and extractive denitrogenation (EDN) [14].

Fourier transform ion cyclotron resonance mass spectrometry (FT-ICR MS) offers the highest available mass resolution, mass resolving power, and mass accuracy, which enable the analysis of complex petroleum mixtures on a molecular level [15]. High-resolution MS data have shown that it is possible to discriminate different compounds [16–18] because of the different ionization efficiencies of the crude oil constituents [19]. In this study, one Brazilian offshore acidic crude oil sample (TAN = 3.19 mg KOH g^{-1}) was submitted to primary characterization using a homemade distillation process (where the boiling points changed from 100.4 to 372.9 °C). Twelve cuts and distillation residues were produced and characterized according to the density, TAN, total sulfur and ESI(±)-FT-ICR MS analyzes. The ESI technique is not suitable to detect neutral aromatic compounds such as sulfur compounds. Thus, the methylation reaction was introduced, and the sulfide compounds were converted from the neutral species to methyl sulfonium salts, which can now be easily transferred into the gas phase in the ESI source [20]. Herein, we apply this approach to investigate the sulfur compound species in the heavy-boiling-point cuts and the distillation residue.

2. Experiment

2.1. Reagents

Anhydrous propan-2-ol, toluene, potassium hydroxide (KOH, analytical grades with purity higher than 99.5%), dichloromethane (CH_2Cl_2), and silver nitrate ($AgNO_3$) were used for the TAN measurements and the methylation reactions. These chemicals were supplied by Vetec Química Fina Ltda, Brazil. Ammonium hydroxide (NH_4OH), sodium trifluoroacetate (NaTFA), formic acid (HCOOH), and methyl iodide (CH_3I) were purchased from Sigma–Aldrich Chemicals USA and used for the ESI(±)-FT-ICR MS measurements. All reagents were used as received.

2.2. Petroleum characterization

A sample of offshore oil from Espírito Santo state (ES), Brazil, were collected in 2011 and used in this work. The oil was characterized according to the standards of the American Society for Testing and Materials (ASTM) by Laboratory of Petroleum Characterization of Federal University of Espírito Santo (LabPetro/UFES-Brazil). A primary characterization was conducted to determine the density (ASTM D5002-99) [21], the API degree (ASTM D1298-99) [22], the total acid number (ASTM D664-09) [23], the kinematic viscosity (ASTM D7042-04) [24], and the total sulfur (ASTM D4294) analyses [25]. Because the emulsified water and sediment value was less than 1.0% v/v, it was not necessary to dehydrate the crude oil sample. The data obtained from the characterization of crude oil are as follows: density = 0.9541 g cm^{-3}, API degree = 16.2, TAN = 3.19 mg KOH g^{-1}, viscosity = 150.45 cSt, at 40 °C, and total sulfur = 0.60 wt% (these information are described in more detail in Table 1).

2.3. True boiling point distillation

A homemade distillation process was implemented in accordance with ASTM D 2892 (Standard Test Method for Distillation of Crude Oil) [26] by LabPetro/UFES (Fig. 1). In general, the laboratorial distillation process (homemade) has the basic principle of operation adopted by the Petroleum Refinery Industry. The main differences relate to loading the crude oil (the refinery operates in a continuum mode, whereas the laboratorial process has been conducted in batches). In other words, the furnace is replaced by a glass flask (Fig. 1). In addition, the differences are related to the heating rate (in the laboratorial process, the heating rate is controlled by an electric mantle).

In the homemade distillation system, the process starts by submitting the dehydrate crude oil to a heating rate (from a distillation flask, see to scheme shown in Fig. 1). The light fraction is vaporized and separated by a column fractionation that contains approximately fourteen to eighteen theoretical plates. After liquefying the gases, the cuts of distillation (from gasoline to diesel) and

Table 1
Physical–chemical characterization of crude oil, its cuts and distillation residue.

Samples	Boiling point range (°C)	Weight (wt%)	Density 20/40 °C	Sulfur content (wt%)	TAN (mg KOH g^{-1})
Cut 1	100.4–170.9	2.15	0.7623	0.02	0.08
Cut 2	170.9–207.5	2.25	0.8207	0.03	0.19
Cut 3	207.5–242.3	2.20	0.8426	0.06	0.45
Cut 4	242.3–262.3	2.13	0.8592	0.09	0.76
Cut 5	262.3–279.4	2.59	0.8704	0.14	1.17
Cut 6	279.4–305.9	2.04	0.8846	0.21	1.36
Cut 7	305.9–315.2	1.90	0.8895	0.26	2.18
Cut 8	315.2–325.0	2.08	0.8959	0,28	3.05
Cut 9	325.0–339.1	2.00	0.9046	0.32	4.13
Cut 10	339.1–354.4	2.18	0.9140	0.38	4.93
Cut 11	354.4–364.2	2.04	0.9201	0.42	5.31
Cut 12	364.2–372.9	2.45	0.9234	0.43	5.43
Crude oil	–	100	0.9541	0.60	3.19
Residue	>372.9	72.60	0.9854	0.71	3.16

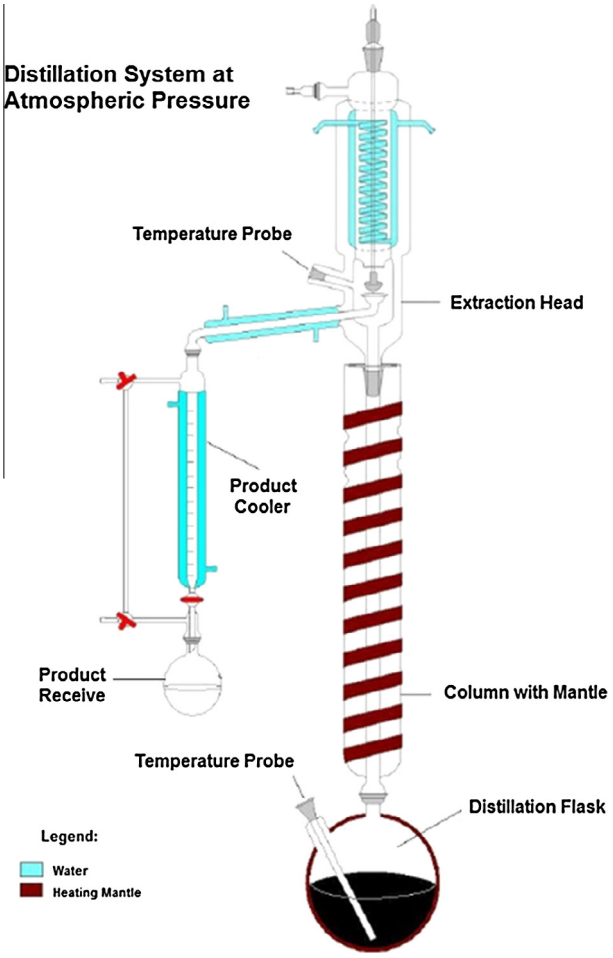

Fig. 1. Illustration of the homemade true boiling point distillation system developed by LabPetro/UFES/Brazil.

the residual oil are produced. The liquefied gases are lost to the atmosphere, whereas the cut distillations are collected in a glass flask located behind the cooler. Finally, the distillation residue remains inside the distillation flask (Fig. 1). Herein, a Brazilian crude oil sample was submitted to a heating rate from 20 to 373 °C at atmospheric pressure and reduced pressures (from 760 to 0.1 mmHg). In the end, this distillation process produced twelve cuts (with the boiling points varying from 100.4 to 372.9 °C) and a final residue with a boiling point above 373 °C. The material balance (weight, *w*,%) was performed for the distillation cuts and the residual oil from the relation in mass values between the crude oil and its respective distillation cuts and residue. Twelve cuts (named cuts 1–12) were extracted according to their mass percentages in the oil source and characterized in terms of the density, TAN, total sulfur and ESI(±)-FT-ICR MS analyses. The density, the total sulfur and the TAN values are shown in Table 1.

2.4. ESI(±)-FT-ICR MS

Petroleum samples were analyzed by both ion modes: positive and negative electrospray ionization, ESI(±). Briefly, the crude oil and the distillation residue samples were diluted to ≈0.4–1.2 mg mL^{-1} and distillation cuts of 0.15 mg mL^{-1} in 50:50 (v/v) toluene/methanol (which contained 0.1% m/v of HCOOH for ESI(+) and NH_4OH for ESI(−)). The resulting solution was directly infused at a flow rate of 5 μL min^{-1} into the ESI source. The mass spectrometer (model 9.4 T Solarix, Bruker Daltonics, Bremen, Germany) was set to operate over a mass range of *m/z* 200–1300. The ESI(±) source conditions were as follows: a nebulizer gas pressure of 0.5–1.0 bar, a capillary voltage of 2.5–4.1 kV, and a transfer capillary temperature of 250 °C. The ion accumulation time in the hexapole was 0.01–0.2 s, which was followed by the transportation to the analyzer cell through the electrostatic lens system. Each spectrum was acquired by accumulating 200 scans of time-domain transient signals in 4 mega-point time-domain data sets. The front and back trapping voltages in the ICR cell were −0.60 V and −0.65 V for ESI(−) and +0.80 V and +0.85 V for ESI(±), respectively. All mass spectra were externally calibrated using a NaTFA solution (*m/z* from 200–1200) after they were internally recalibrated using a set of the most abundant homologous alkylated compounds for each sample. A resolving power ($m/\Delta m_{50\%} \approx 500{,}000$, in which $\Delta m_{50\%}$ is the full peak width at half-maximum peak height) of *m/z* 400 and a mass accuracy of <1 ppm provided the unambiguous molecular formula assignments for singly charged molecular ions. The mass spectra were acquired and processed using a custom algorithm developed specifically for petroleum data processing, Composer software (Sierra Analytics, Pasadena, CA, USA). The MS data were processed, and the elemental compositions of the compounds were determined by measuring the *m/z* values. To help visualize and interpret the MS data, a typical plot was constructed, such as a carbon number versus the double bond equivalents (DBE), where DBE is defined as the number of rings plus the number of double bonds in a molecular structure. The aromaticity of a petroleum component can be deduced directly from its DBE value according to the following equation:

$$\mathrm{DBE} = c - h/2 + n/2 + 1 \quad (1)$$

where *c*, *h*, and *n* are the numbers of carbon, hydrogen, and nitrogen atoms, respectively, in the molecular formula.

2.4.1. ESI(±)-MS/MS

Tandem mass spectrometry (MS^n) experiments were performed on a linear quadrupole ion-trap, LTQ, (Thermo Scientific, Bremen, Germany). The spectra were collected in ESI(+) and ESI(−) using a max ion source (Thermo Scientific, Bremen, Germany). The typical ESI conditions were: (i) *n* infusion flow rate at 2 μL min^{-1}; (ii) a nebulizing temperature of 240 °C; (iii) a sheath gas flow of 16 (arbitrary unit); (iv) an auxiliary gas flow of 5 (arbitrary unit); (v) and an *iso* spray voltage of 3.10 kV. Other experimental parameters for ESI(+) and ESI(−) sources were used are, respectively: (vi) capillary temperature of 220 °C; (vii) tube lens of 120 and −100 V; and (viii) capillary voltage: 35 and −39 V. The ESI(±)MS/MS spectra were acquired with automatic gain control averaging 5 microscans for each spectrum with isolation window of 1.0 (*m/z* units) and 25–45% of the collision energy. The spectra were processed using the Xcalibur Software (Thermo Scientific, Bremen, Germany).

2.4.2. Methylation reactions

The methylation procedure for sulfur compounds has been reported in 2010 and 2011 by Liu et al. [27,28] Herein, the methylation reactions (Fig. 2) were performed only for heavy distillation cuts such as cuts 11 and 12 and the residual oil because of the high sulfur content (0.42, 0.43 and 0.71 wt%, respectively (Table 1)). First, 100 mg of samples were weighted and dissolved in a solution of methyl iodide (0.1 mmol mL^{-1} in dichloromethane) under continuous stirring. Afterwards, an alcoholic solution containing 1.0 mmol of silver nitrate was added, and a yellow precipitate silver iodide was spontaneously formed (silver iodide, see Fig. 2). The reaction remained under a reduced pressure and constant stirring during 48 h. Finally, the formed precipitate was removed by centrifuge and filtration, and the remaining solution, which contained sulphonium salts (Fig. 2), was evaporated to ensure a total removal of impurities such as methyl iodide and dichloromethane. The produced sulphonium salts were analyzed using ESI(+)-FT-ICR MS.

3. Results and discussion

The physical–chemical characterization (boiling point, weight, density, total sulfur and TAN) of crude oil and its respective distillation cuts and residue is shown in Table 1. For the crude oil distillation cuts, the total sulfur and TAN values increase by thirty and seventy times, respectively, when the boiling point increases. The result is mainly evident when we compare the values obtained for cut 1 (*S* = 0.014 wt% and TAN = 0.077 mg KOH g^{-1}) and cut 12 (*S* = 0.43 wt% and TAN = 5.43 mg KOH g^{-1}). When the light fractions, which contain mainly hydrocarbons, are removed from the crude oil, an increase of the *S* content is also observed from the crude oil to its distillation residue (0.60 → 0.71 wt%). However, a little reduction in the TAN values is observed (3.19 → 3.16 mg KOH g^{-1}). For sulfur heteroatom compound species (S_x classes, where *x* = 1–3), this reduction is due to the higher thermal stability in comparison with the naphthenic acids species. This last can experience thermal-degradation reactions during the distillation process and produce low chain length naphthenic acids (C_1–C_4), which are improved by its low aromaticity (maximum of DBE ≅ 4) [29,30] and low boiling point or can also undergo decarboxylation reactions as a consequence of this poor thermal stability [31,32].

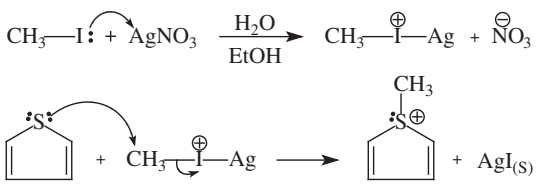

Fig. 2. Methylation reactions.

3.1. ESI(-)-FT-ICR MS

Fig. 3a shows the ESI(-)-FT-ICR mass spectra for cuts 1–12, which were extracted by the laboratorial petroleum distillation system, where the naphthenic acids species are detected as deprotonated molecules: $[M–H]^-$ ion. In the light distillation cuts such as cut 1, the ESI(-)-FT-ICR mass spectrum identifies only ions that correspond to the impurities from the background: $[C_{15}H_{24}O–H]^-$: *m/z* 219.1755, $[C_{16}H_{32}O_2–H]^-$: *m/z* 255.2330, $[C_{18}H_{32}O_2–H]^-$: *m/z* 279.2330 and $[C_{18}H_{34}O_2–H]^-$: *m/z* 281.2487, which most likely correspond to butylated hydroxytoluene, and palmitic, linoleic and oleic acids, respectively. These ions do not represent the typical homologous series observed for naphthenic acid as shown in the ESI(-)-FT-ICR mass spectra (see cuts 2–12). Additionally, these impurities are also detected in the other light crude-oil cuts (cuts 1–4), where the naphthenic acid concentration is low (TAN values vary from ≅0.08 → 0.76 mg KOH g^{-1}) and disappears with the increase in the distillation cut temperature. In general, the presence of naphthenic acids with low *m/z* cannot be disregarded because of the width of the bulk of light distillation cuts such as cut 1 (mainly, the linear naphthenic acid that contains a number carbon varying from C_1 to C_7). An alternative to identify these light acids species with a low boiling point *T* < 171 °C and *m/z* < 150 is to use the other MS analyzers (such as quadrupole, ion traps, TOF or Orbitraps) or other analytical techniques (ion chromatography [33] and electrophoresis capilar).

The ESI(-)-FT-ICR mass spectra from cuts 2 to 12 show the detection of 122 naphthenic acid species with *m/z* ranging from 153 to 421 (see Fig. 3a and Table 1S (Supplementary material)). Table 1S shows the predicted molecular formulas and their possible chemical structures from the measured and theoretical *m/z* values, the DBE and the mass error (which is generally lower than 1 ppm). These results are summarized in Fig. 4. Note that besides the naphthenic acid species that are the majority, phenol analogue species (O1 Class, DBE = 4)) are also detected with *m/z* ranging from 163 to 357, DBEs from 4 to 5 and carbon number from C_9 to C_{25}. When the distillation cut temperature increases, the amounts of O2 species (O2 class) or naphthenic acids also increase (from 9 compounds for cut 2 to 66 compounds for cut 12), and the average molecular weight distribution, M_w, shifts to higher *m/z* values (M_w = 169 → 321 Da) (Fig. 3a). These results are consistent with previously results obtained by Marshall et al. [34]. Moreover these results match with the increasing of TAN as the boiling point increases (Table 1) [24].

One method to display the similarities or differences between the signal patterns of the crude oil samples and the distillation cuts is to construct certain types of plots such as the plots of DBE versus the carbon number. These plots have proven to be useful tools to differentiate complex organic mixtures based on the chemical composition [35,36], which shows the distribution of all components from a specific class. Each line in the diagram represents a homologous series with a specific DBE value (Fig. 3b).

Fig. 3b shows the plots of the DBE versus the carbon number for the O2 class of distillation cuts (cuts 1–12), which contain compounds with DBEs ranging from 1 to 9 and carbon numbers ranging from C_9 to C_{26}. For distillation cuts 2 and 3, the most abundant compounds show a carbon number of C_{10}–C_{11} with a constant DBE of 2 (M_w = 169–183 Da). These species are mainly composed of one naphthenic ring (five- or six membered) and one carboxyl group. For the other distillation cuts (cuts 4–12), the maximum abundance is located for high carbon numbers (varying from C_{12}

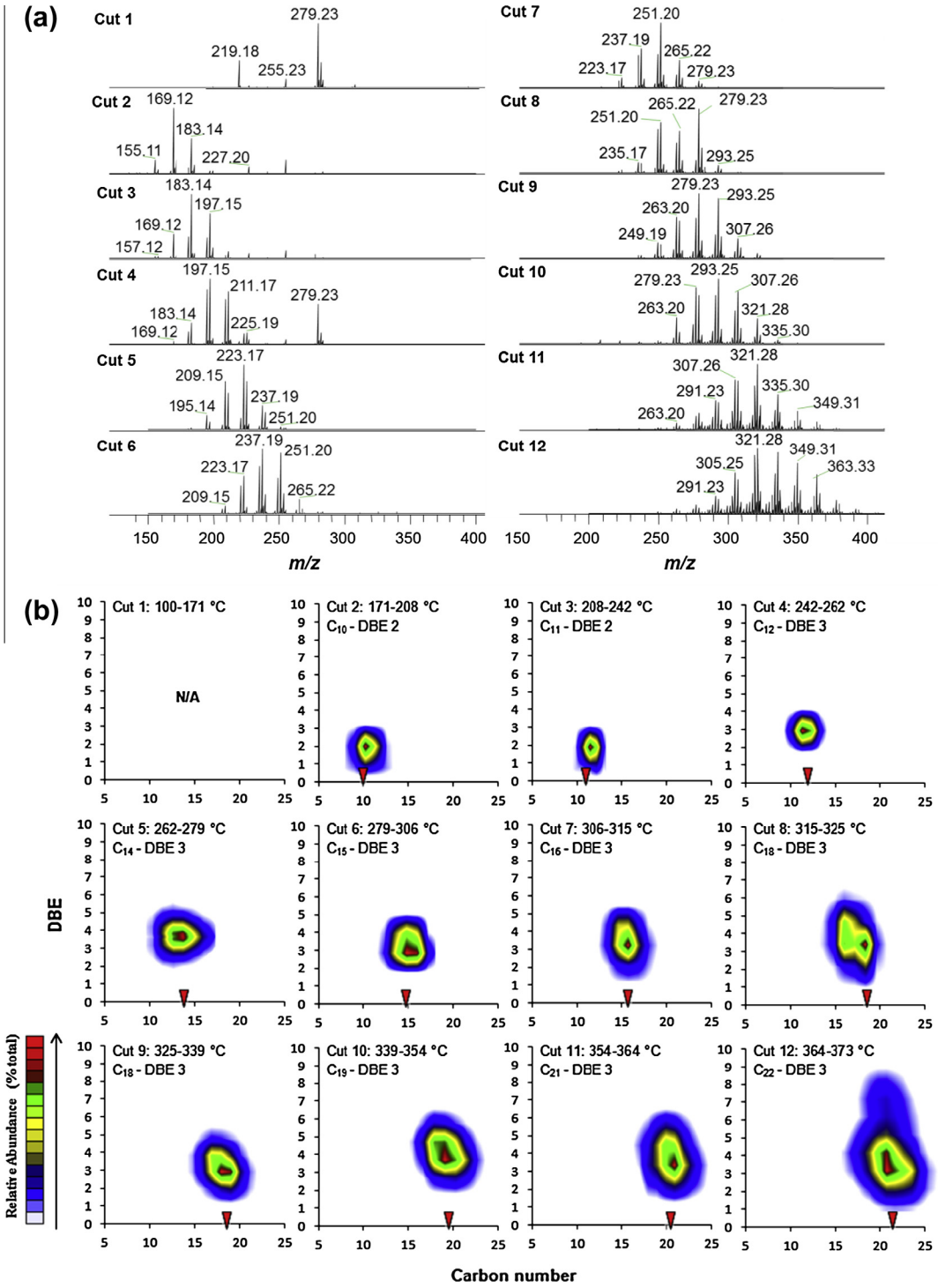

Fig. 3. (a)ESI(−)-FT-ICR MS for the distillation cuts and (b) plots of DBE versus carbon number for the O2 class of distillation cuts.

to C_{22}) with a constant DBE of 3, which is now composed of two naphthenic rings and one carboxyl group (see the proposed structure in Fig. 4 and Table 1S).

Some studies in literature report the correlation between the chemical composition of crude oil and the corrosion process [24,37]. In 2012, Huang et al. [29] studied the synergy effect of naphthenic acid corrosion and sulfur corrosion at high temperature (280 °C) in a crude oil distillation unit using Q235 carbon–manganese steel and 316 stainless steel. In a corrosion media containing only sulfur (from 1 to 5 wt%), the corrosion rate of Q235 and 316 first increased and then decreased with the increasing of sulfur content. However, when the naphthenic acid and the sulfur compounds were added together (in the first case, the TAN ranged from 3 to 15 mg KOH g^{-1} with S of 1 wt%, and in the second case, TAN = 6 mg KOH g^{-1}, and S ranged from 1 to 5 wt%), a synergy effect on the corrosion rate was observed in Q235 and 316. In the same year, Freitas et al. [24] studied the effect of composition of heavy distillation cuts from heavy crude oil (density = 0.93 and TAN = 1.93 mg KOH g^{-1}) on the corrosion process. The cuts with boiling temperatures lower than 315 °C and

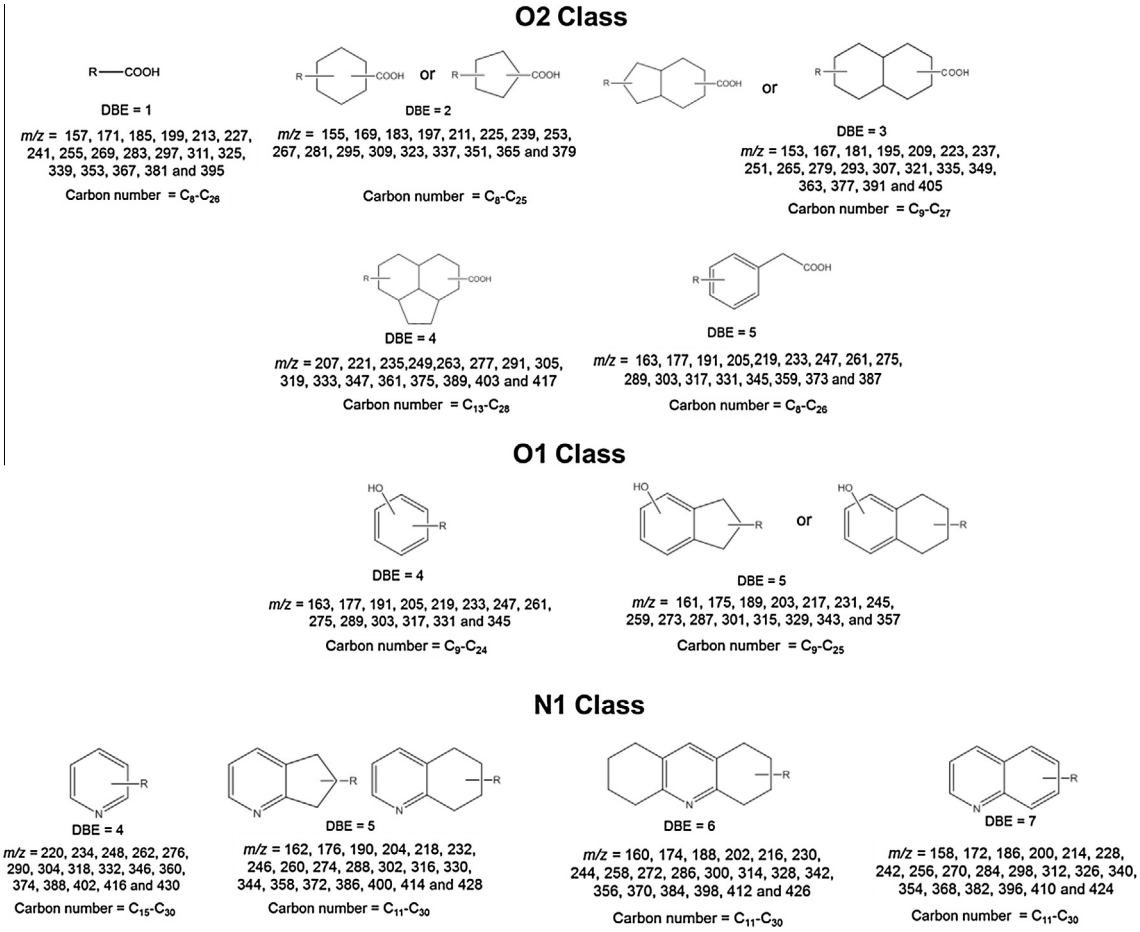

Fig. 4. Possible chemical structures for O2, O1 and N classes present in the crude oil distillation cuts, which contain their respective DBE, *m/z* and carbon number values.

TANs (ranging from 0.47 to 1.83 mg g^{-1}) were studied. According to the ESI(-)-FT-ICR MS results, the naphthenic acid species were detected in the six cuts studied (cuts 2–7), with $m/z < 300$ and DBEs ranging from 2 to 4. Similarly, the relative abundance of heavy naphthenic acids and the TAN increase with the distillation cut temperature. This information correlated with the corrosion mechanism for AISI 1020 steel in the heavy oil and the distillation cuts, where the corrosion was more evident in the oil distillation cuts that were characterized as alveolar and pitting. In addition, Piehl [38] and Slavcheva et al. [39] show that the corrosion rate had increased (from 0.30 mm/y to 1.27 mm/y) as a function of boiling point (from 204 °C to 371 °C) for cuts with TAN ≅2 mg KOH g^{-1}. It also increased (from 1.27 mm/y to 2.08 mm/y) as a function of TAN (from 2 mg KOH g^{-1} to 10 mg KOH g^{-1}) at 371 °C [40]. Therefore, it is expected that the heavy distillation cuts will be more corrosive than the light distillation cuts. In other words, the corrosion rate will increase in the following order: naphtha (cuts 1–2) < kerosene (cuts 3–4) < gas oil (cuts 5–12). Additionally, the corrosion process can be contributed by the sulfur compound species [29], which mainly present in the heavy distillation cuts (cuts 5–12) (Table 1).

Finally, alternative methods have recently been developed to reduce the amount of naphthenic acid species and consequently the corrosion rate [41,42,31]. These processes normally involve critical and expensive conditions such as high temperatures (300–400 °C) and an inert N_2 atmosphere [33], the use of supercritical water in a batch reactor at 500 °C and 50 MPa [34], or thermal cracking and catalytic decarboxylation over alkaline earth-metal oxides and ZnO catalysts [35].

Fig. 5a and b shows the ESI(-)-FT-ICR mass spectra for the crude oil (5a) and its respective distillation residue (5b), with *m/z* range from 200 to 1000, which correspond primarily to naphthenic acids and carbazole analogue species. An expansion in the *m/z* region of 400–410 allows the comparison of the relative intensity of the two main species identified (the insets in Fig. 5a and b). Note that the relative abundance of the heavy naphthenic acids decreases from the crude oil to its residue distillation. This reduction is due to the migration of light species during the distillation process from the crude oil studied to the cuts; consequently, the M_w is shifted and broadened to high values (603 Da → 627 Da[1]). It is more evident when we analyze the plots of DBE versus carbon number for the O2 and N classes of crude oil (Fig. 5c–e) and its residue distillation (Fig. 5d–f). Both classes are affected by the atmospheric distillation process. Initially, the high abundance of hydrocarbon homologous series of polar markers for the N class ranged from C_{34} (Fig. 5c, crude oil) to C_{44} (Fig. 5d, residue distillation), with the maximum DBE constant in aromaticity, DBE = 14. It is due to the ionic suppression phenomenon, which is caused by removing the naphthenic acids with carbon numbers than lower C_{20} from the crude oil and dissolving them along the distillation cuts at temperatures between 100 and 373 °C (see the highlighted area in bold in the region of number carbon between C_{10} and C_{20}, Fig. 5e and f). Generally, for the O2 class, the maximum values of the abundance distribution remained constant: C_{31} and DBE 3. These results are similar to reported in the literature [43].

[1] M_w was obtained from the petroleum data processing using Composer software, where ≅92% signals were assigned.

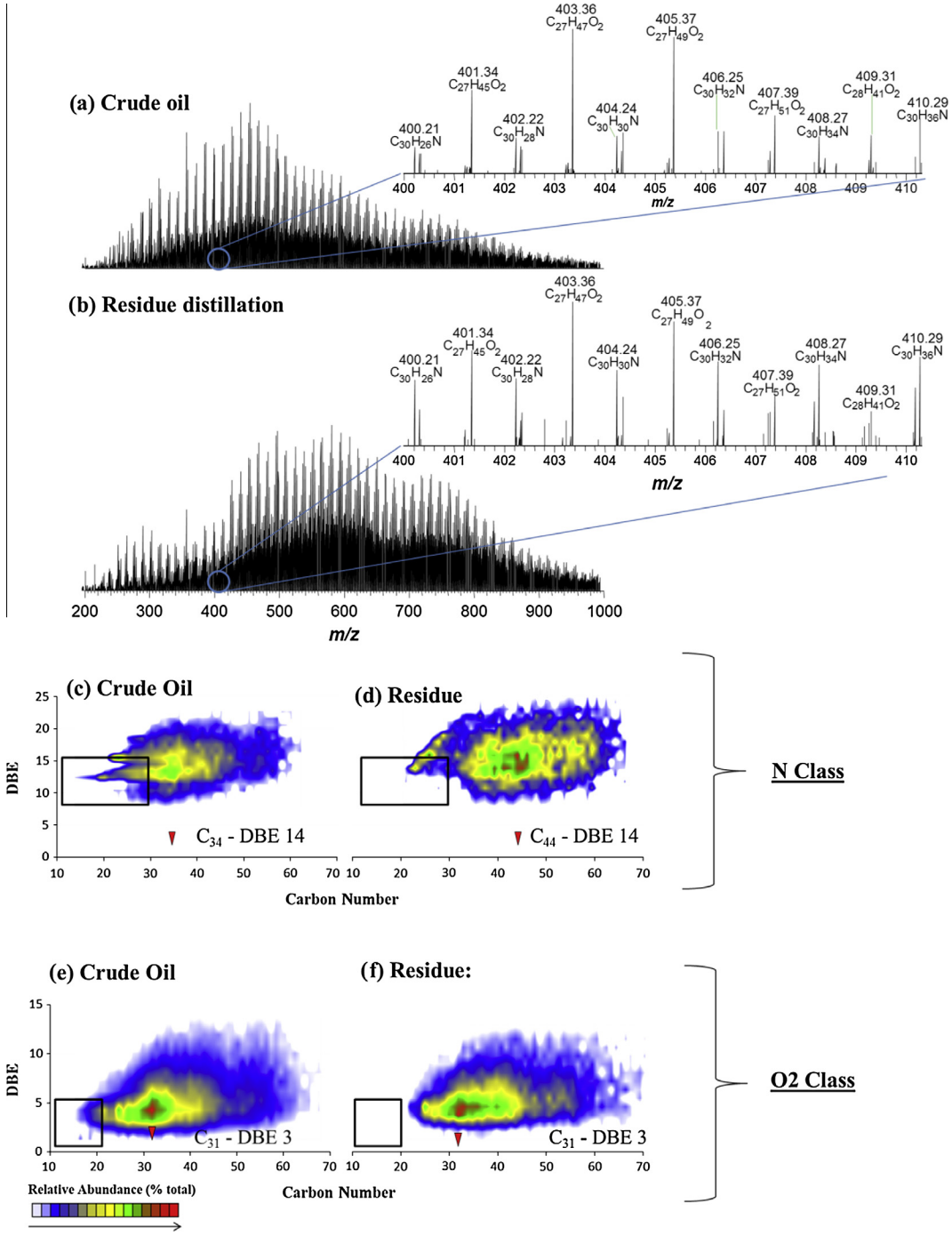

Fig. 5. ESI(−)-FT-ICR MS for (a) crude oil and (b) residue distillation; plots of DBE versus carbon number for the N and O2 classes that correspond to (c–e) the crude oil and (d–f) the residue distillation. The carbon number abundance distribution maximum (red arrow) shifts from ≈C_{34} (crude oil, 3c) to ≈C_{44} (residue distillation, 3d) for the N class. The DBE values remained constant in aromaticity: DBE = 14. For the O2 class, the maximum values of the abundance distributions remained constant: ≅C_{31} and DBE = 3. (For interpretation of the references to colour in this figure legend, the reader is referred to the web version of this article.)

3.2. ESI(+)-FT-ICR MS

Similar to the ESI(-)-FT-ICR MS results, the ESI(+)-FT-ICR mass spectra for the distillation cuts 1–12 (Fig. 6a and b), the crude oil and its residue (Fig. 7a–d) are shown. Now, the polar species from pyridine derivatives (Nx class) are detected as the protonated molecules: $[M + H]^+$ ion. Again, for the light distillation cuts (cut 1), the ESI(+)-FT-ICR mass spectrum identifies the ions corresponding to impurities such as *m/z* 301 (which originated from methanol that is used in the preparation of the solution). For the other cuts (cuts 2–12), the ESI(+)-FT-ICR mass spectra show the detection of ≅100 compounds (the number is lower than that observed for the naphthenic acidic species). These species show *m/z* ranging from 160 to 414 (Fig. 6a). Table 2S (Supplementary material) shows the predicted molecular formulas and their possible chemical structures of most pyridine derivative species, which are obtained from the measured and the theoretical *m/z* values, DBE and mass error. The results are summarized in Fig. 4. Note that when the distillation cut temperature increases, the amount of nitrogen species identified (N class) increases, and the M_w shifts toward higher

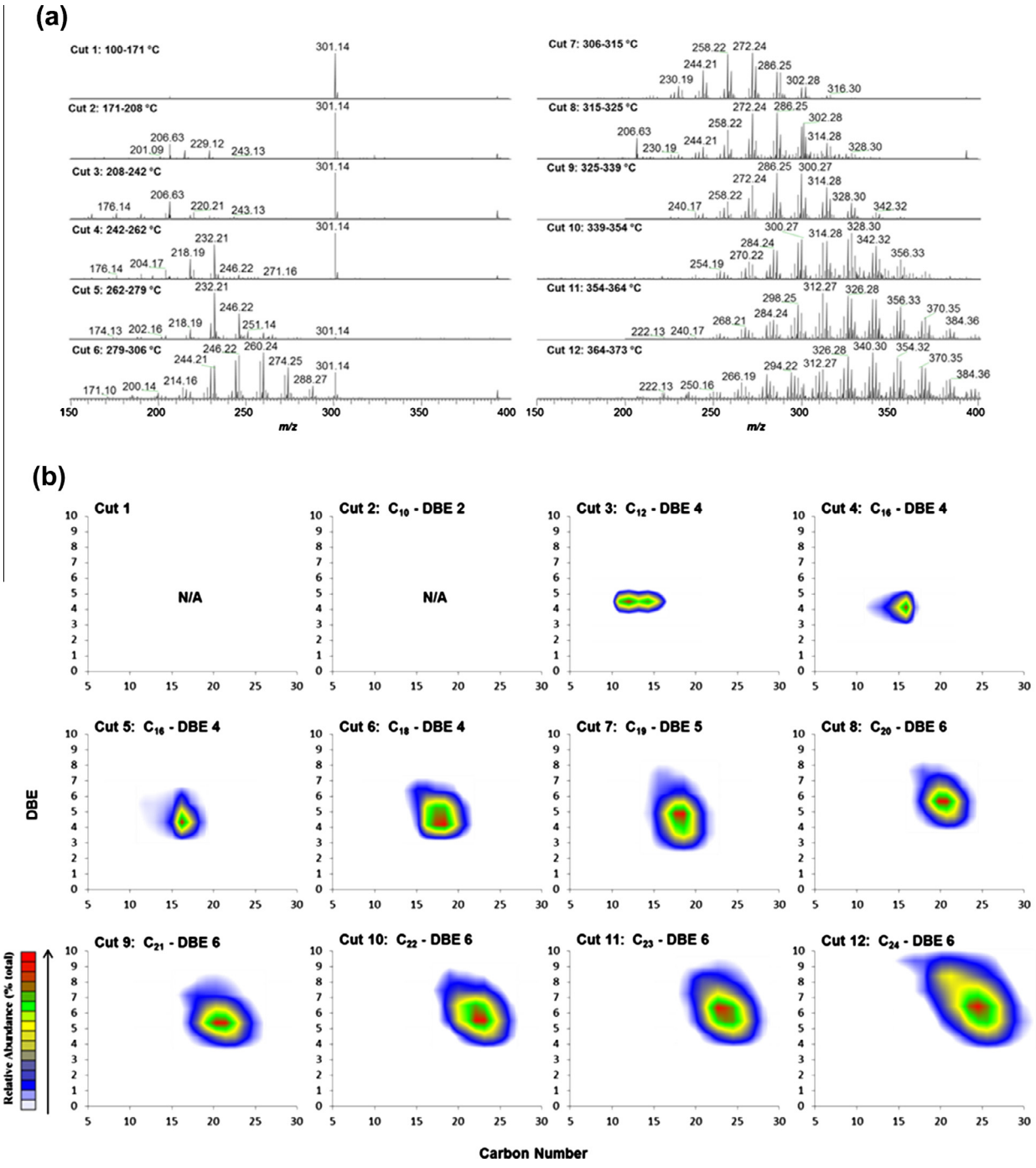

Fig. 6. (a) ESI(+)-FT-ICR MS for the distillation cuts: detection of ≅100 pyridine derivative species that show *m/z* ranging from 160 to 414; (b) plot of DBE versus carbon number for the N class: for the light distillation cuts (3–6), the most abundant compounds show carbon numbers of C_{12}–C_{18} with DBE = 4; whereas for the heavy distillation cuts (8–12), we observed carbon numbers of C_{20}–C_{24} and DBE = 6.

values (6 species and M_w = 206 Da for cut 3; and 64 species and M_w = 340 Da for cut 12) (Fig. 6a).

Fig. 6b shows the plots of the DBE versus the carbon number for the N class of distillation cuts (cuts 1–12), which there are compounds with DBEs ranging from 3 to 10 and carbon numbers ranging from C_{11} to C_{29}. For distillation cut 3, the most abundant compounds show a carbon number of C_{12} and a constant DBE of 4. These species are mainly composed of one pyridine ring (six membered containing an N atom) and one alkyl group (R) (Fig. 4). For the other distillation cuts (cuts 8–12), the maximum abundance is located at high carbon numbers (changing from C_{20} to C_{24}) with a constant DBE of 6, which is now composed of one pyridine ring and two naphthenic ring (five- or six-membered).

Fig. 7a and b shows the ESI(+)-FT-ICR mass spectra for crude oil (7a) and its respective distillation residue (7b), where *m/z* ranges from 200 to 1000. Generally, the M_w is subtlety shifted and broadened to high values (≅500 Da → 550 Da), which is more evident when we compare the plots of DBE versus carbon number for the pyridine derivative species (N class) of crude oil (Fig. 7c) and its residue distillation (Fig. 7d). The high abundance hydrocarbon homologous series of polar markers for the N class ranges from C_{35} (Fig. 7c, crude oil) to C_{40} (Fig. 7d, residue distillation), and the

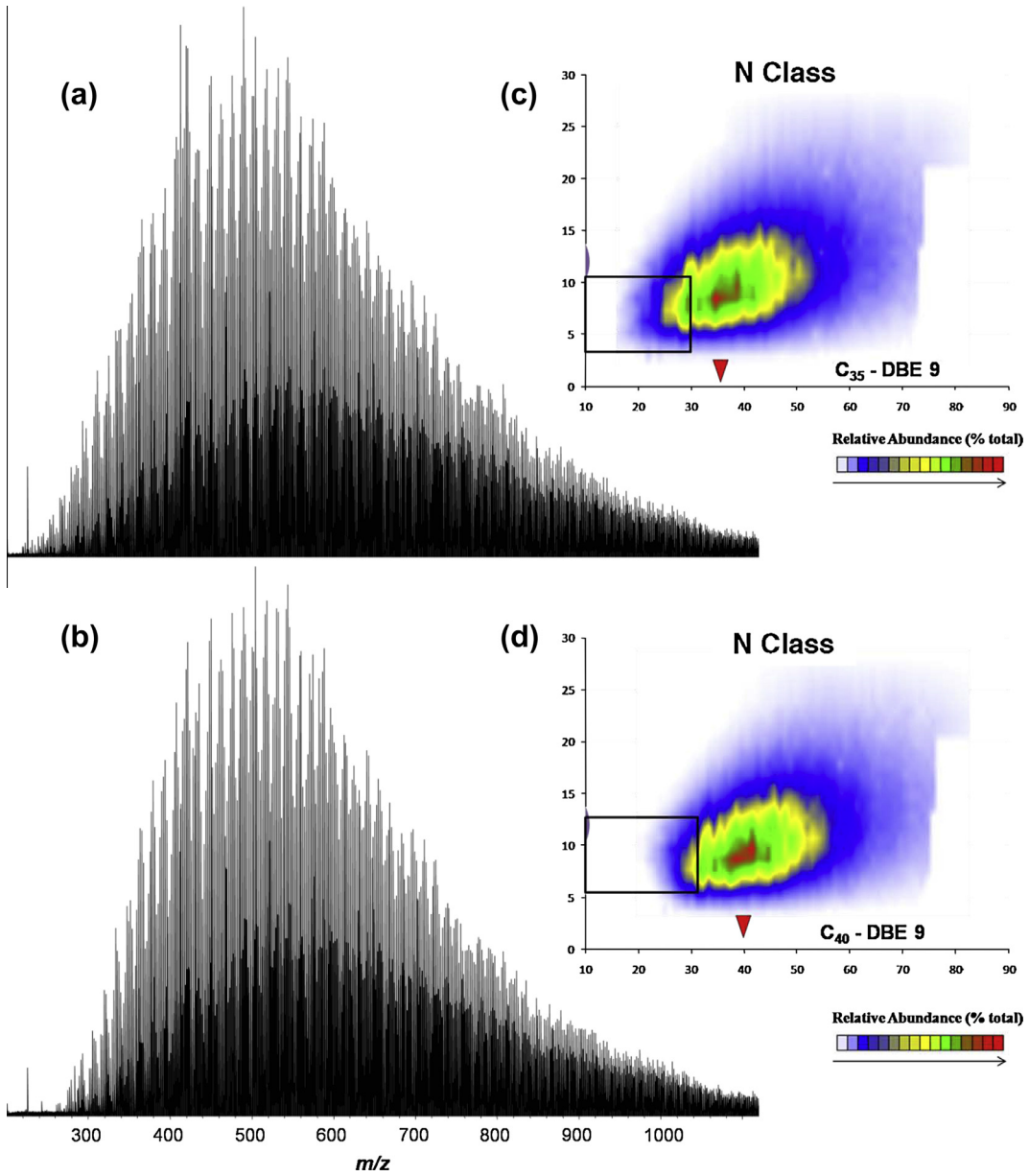

Fig. 7. ESI(+)-FT-ICR MS for (a) crude oil and (b) residue distillation; plots of DBE versus carbon number for the N class of (c) crude oil and (d) its residue distillation.

maximum DBE is constant in aromaticity: DBE = 9. The result is due to the removal of nitrogen species with low chain length (from C_{11} to C_{29}) from the crude oil during the atmospheric distillation process (see the highlighted area in bold in the region of number carbon between C_{10} and C_{30} in Fig. 7c and d).

For both oils, the N compound class is the most abundant class (≅90%). The N2 class is the second most abundant (≅7%), followed by the NO class (≅3%). The distillation process removes primarily nitrogen compound species (N class) from the crude oil to the distillation cuts (Fig. 6), and consequently, a small decrease in the relative intensity of the N class (90 → 88%) and an increase of the N2 class (7 → 9%) is observed.

3.3. Methylation reaction

Fig. 8a–c shows the ESI(+)-FT-ICR mass spectra for the heavy distillation cuts (cuts 11 and 12, 8a and b) and the distillation residue (8c) derived from methyl sulfonium salts with M_w = 326, 340 and 767 Da, respectively. An expansion in the *m/z* regions of *m/z* 316–340 (8a), *m/z* 360–380 (8b) and *m/z* 730–740 (8c) summarizes the identification of the presence of sulfur class species. A total of 51, 53 and 304 sulfur species were detected from distillation cuts 11, 12 and the residue. Note that the basic nitrogen class species are also identified due to the lower pKa values (pKa ≅ 5.3) (Fig. 8a and b) when compared to the sulfur class species (benzothiophene, pKa ≈ 33 and thiols groups, pka ≈ 10.5). In all cases, the presence of the S1 class is observed to correspond to sulfides and thiophenic compounds.

The S1 class can be visualized similarly to the plots of the DBE versus the carbon number of the heavy distillation cuts (cuts 11, and 12, Fig. 9a and b) and the distillation residue (Fig. 9c). For the heavy distillation cuts, there are compounds with DBEs ranging from 0 to 6 and carbon numbers ranging from C_{18} to C_{30}. The most abundant compounds show carbon numbers of C_{23} (for cut 11) and C_{25} (for cut 12) with a constant DBE of 3 (Fig. 9a and b). For the distillation residue, DBEs and carbon number ranging from 0 to 8 and C_{35} to C_{70}, respectively, were observed with maxima of DBE = 4 and C_{43} (Fig. 9c).

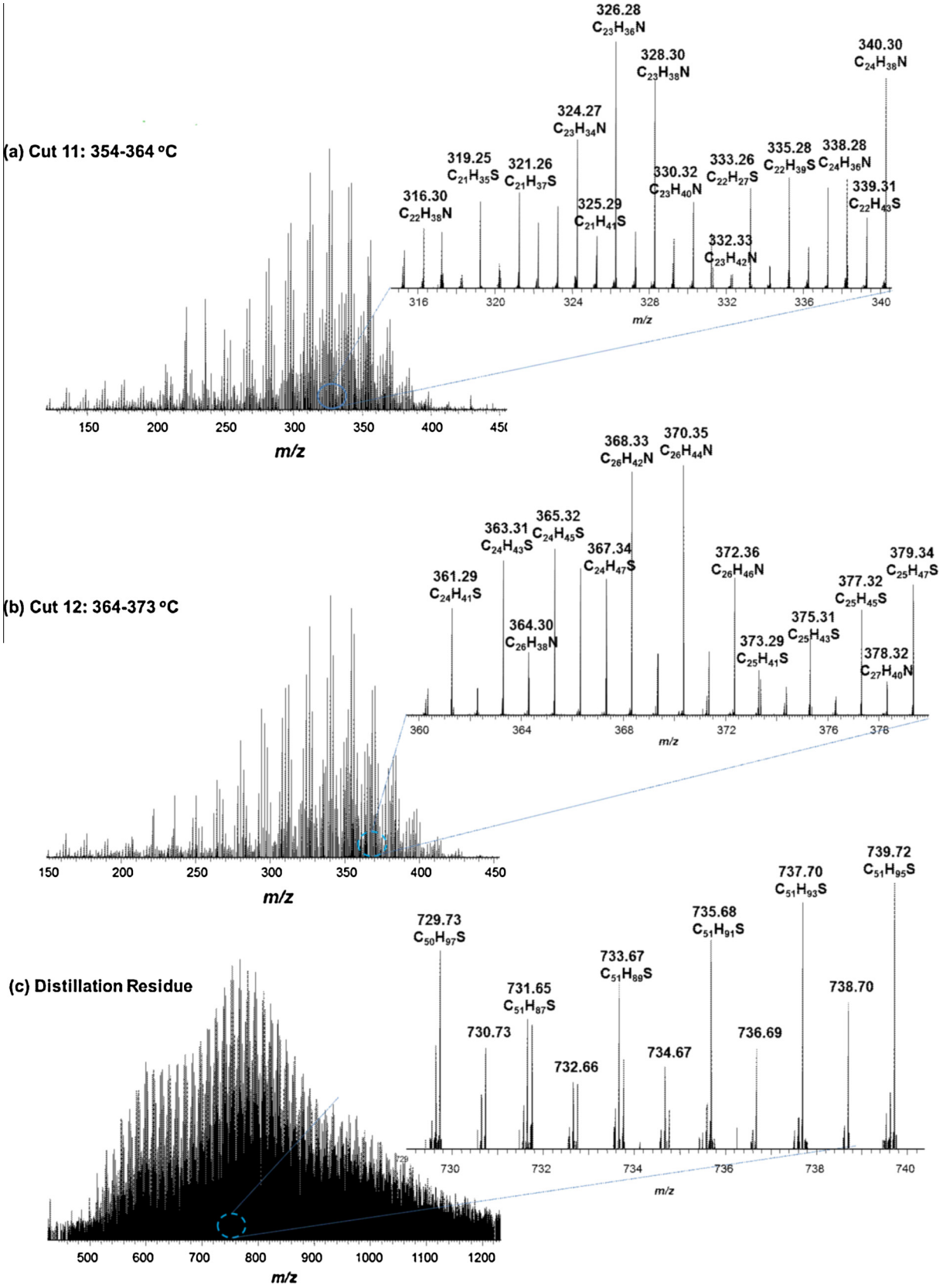

Fig. 8. ESI(+)-FT-ICR MS spectra for cuts (a) 11 and (b) 12, and (c) distillation residue derived from methyl sulfonium salt.

In 2011, Liu et al. [22] studied the elemental composition and distribution of sulfide and thiophenic compounds in four subfractions of Kazakhstan vacuum gas oil (the simulated distillation curves of the VGO subfractions ranged from 150 to 600 °C). The samples had M_w ranging from 250 to 500 Da with the S1 class species being the majority, where DBE values $\geqslant 6$ are likely thiophenic compounds, whereas those with DBE values $\leqslant 6$ are sulfides. Therefore, for the heavy distillation cuts and residue, the sulfide class

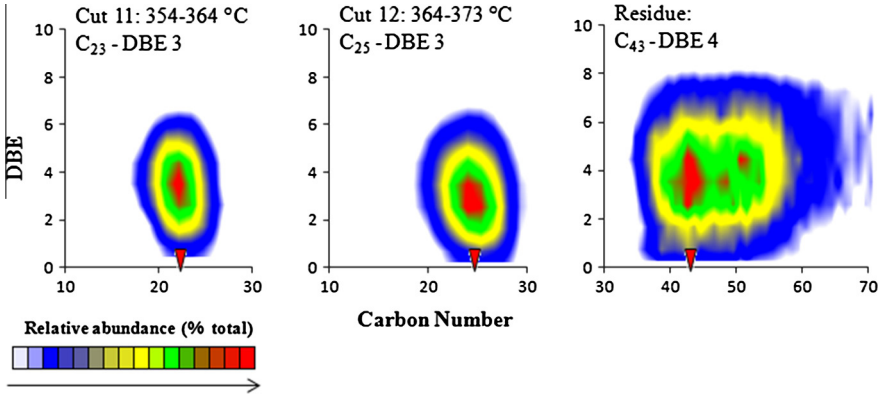

Fig. 9. Plots of DBE versus carbon number for S1 class of heavy distillation cuts (cuts 11 and 12) and distillation residue derived from methyl sulfonium salts.

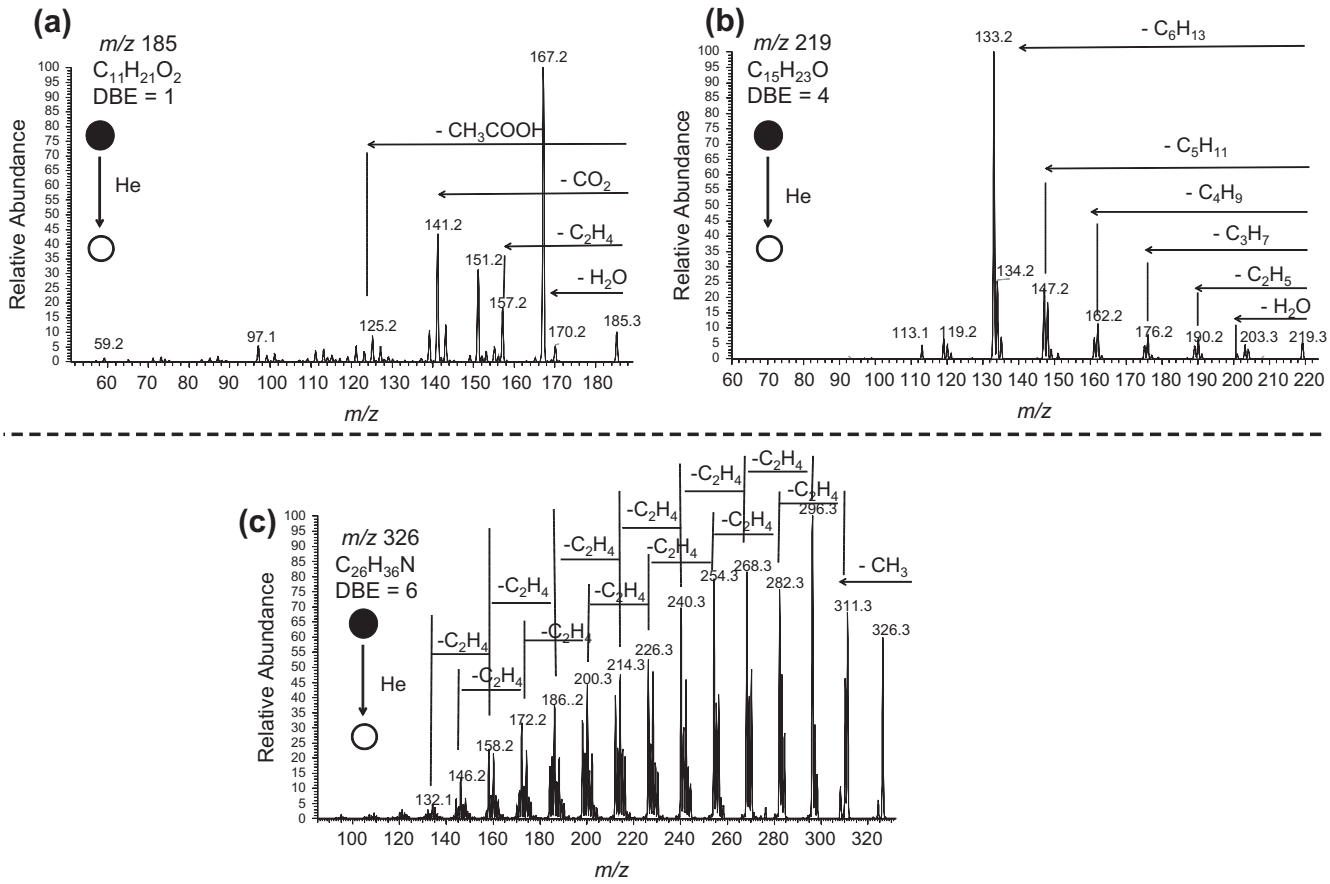

Fig. 10. ESI(±)-MS/MS spectra of typical (a) O2, (b) O and(c) N compound classes.

species are the majority. The sulfur compounds with DBE = 0 are aliphatic sulfides. Those with DBEs =1 and 2 are one- and two-cyclic-ring sulfides, respectively. For the S1 class, the species with DBE =3 are likely tricyclic-ring sulfides. The S1 class species with DBEs $\geqslant$4 are likely cyclic-ring or aromatic sulfides. The S1 class species with DBEs $\geqslant$6 are presents only in the distillation residue and correspond to benzothiophene and dibenzothiophene compounds [9,22]. In 2010, the same group [21] worked in methylsulfonium salt characterization in crude oil and its fractions (saturates, aromatics, resins, and asphaltenes). For crude oil and its light fractions (saturates and aromatics), the S1 class had the highest relative intensity, which is in good agreement with our results. Additionally, the other sulfur class species were also identified (S2, O2S1, O1S1, N1S1, S3, O1S2 and O2S1).

3.4. ESI(±)-MS/MS

To confirm the structures and the connectivity of some compound classes that are more abundant (O2, O and N classes), which were identified using ESI(±)-FT-ICR MS, the ESI(−)-MS/MS spectra were acquired for the ions $[C_{11}H_{22}O_2–H]^-$ and $[C_{15}H_{24}O–H]^-$ of *m/z* 185.1549 and 219.1755 and ESI(+)-MS/MS for ion

$[C_{26}H_{35}N + H]^+$ of *m/z* 326.2840 (Fig. 10a–c). This approach identifies the characteristic loss and confirms the existence of O2 compounds such as the carboxylic acids, O compounds such as phenolic alkylated (which has DBE = 4), and N compounds such as the pyridinic derivatives.

Initially, for Fig. 10a, the CID experiment of ion $[C_{11}H_{22}O_2–H]^-$ of *m/z* 185.1549 produces fragments with *m/z* 167, 141 and 125, which correspond to the neutral losses of 18 Da (H_2O), 44 Da (CO_2) and 60 Da (acetic acid, CH_3CO_2H), respectively. Meanwhile, the ESI(−)MS/MS of the ion $[C_{15}H_{24}O–H]^-$ of *m/z* 219.1755 produces fragments of *m/z* 201 (via neutral loss of H_2O) and a series of signals (m/z 190, 176, 162, 147 and 133), which are attributed to the alkyl chain fragmentation (Fig. 10b). These fragmentation patterns allow for the identification of phenolic derivative species (O1 class) with DBE = 4, where its alkyl chain varies as a function of the carbon number. Finally, for the ESI(+)MS/MS spectrum of ion $[C_{26}H_{35}N + H]^+$ of *m/z* 326.2840, a classic fragmentation pattern of the alkyl chain is observed (in most cases, the neutral loss of C_2H_4 and 28 Da are observed), which is proposed to represent a pyridinic ring and a large alkyl chain (Fig. 10c).

4. Conclusion

Electrospray ionization Fourier transform ion cyclotron resonance mass spectrometry (ESI(±)-FT-ICR MS) had been demonstrated as a powerful analytical tool in the chemical typification of polar compound species. For oxygen-containing species, the ESI(−)-FT-ICR MS spectra showed the detection of 122 naphthenic acid species in the distillation cuts with *m/z* ranging from 153 to 421. When the distillation cut temperature increased, the amount of O2 species increased (from 9 for cut 2 to 66 for cut 12), and the average molecular weight distribution, M_w, shifted to higher *m/z* values (M_w = 169 → 321 Da). These results were consistent with the increase of TAN with the boiling point. The plots of the DBE versus the carbon number for the O2 class for the heavy distillation cuts (cuts 4–12) suggested a maximum abundance for the carbon numbers of C_{12}–C_{18} with a constant DBE of 3. The basic structure of these species is composed of two naphthenic rings and one carboxyl group. The phenol analogue species were also detected (O1 Class, DBE = 4–5) with *m/z* ranging from 163 to 357 and carbon number ranging from C_9 to C_{25}. For the ESI(+)-FT-ICR MS spectra, approximately 100 nitrogen compound species were detected with *m/z* ranging from 160 to 414. Similar to the ESI(−)-FT-ICR results, the amount of nitrogen species increased, and the M_w shifted for high values (6 species and M_w = 206 Da for cut 3; and 64 species and M_w = 340 Da for cut 12). The structures and the connectivity of naphthenic acids, phenols and pyridines were confirmed using ESI(±)-MS/MS, where the typical neutral losses were detected such as 18 Da, 44 Da and 60 for naphthenic acid and 18 Da for phenolic derivative species. A classic fragmentation pattern corresponding to the alkyl chain was observed for the pyridine species.

Methylation reactions have been demonstrated as an efficient analytical method to detect sulfur compound species. The most abundant compounds in the heavy distillation cuts presented C_{23} (for cut 11) and C_{25} (for cut 12) with a constant DBE of 3. For the distillation residue, the maxima of DBEs and the carbon number were DBE = 4 and C_{43}. These results suggested the presence of sulfide class species as the majority structure (cyclic-rings or aromatic sulfides), i.e., the S1 class.

Appendix A. Supplementary material

Supplementary data associated with this article can be found, in the online version, at http://dx.doi.org/10.1016/j.fuel.2013.07.008.

References

[1] (a) Hughey CA, Rodgers RP, Marshall AG, Walters CC, Qian K, Mankiewicz P. Acidic and neutral polar NSO compounds in smackover oils of different thermal maturity revealed by electrospray high field Fourier transform ion cyclotron resonance mass spectrometry. Org Geochem 2004;35:863–80;
(b) Hughey CA, Rodgers RP, Marshall AG, Qian K, Robbins WK. Identification of acidic NSO compounds in crude oils of different geochemical origins by negative ion electrospray Fourier transform ion cyclotron resonance mass spectrometry. Org Geochem 2002;33:743–59.

[2] Marshall AG, Rodgers RP. The next grand challenge for chemical analysis. Acc Chem Res 2004;37:53–9.

[3] Brient JA. Commercial utility of naphthenic acids recovered from petroleum distillates. In: Symposium on acidity in crude oil, presented before the division of petroleum chemistry, Inc., 215th National Meeting, American Chemical Society, Dallas, TX, March 29-April 3; 1998.

[4] Barrow MP, Headley JV, Peru KM, Derrick PJ. Data visualization for the characterization of naphthenic acids within petroleum samples. Energy Fuels 2009;23:2592–9.

[5] Wu Z, Rodgers RP, Marshall AG. Compositional determination of acidic species in Illinois #6 coal extracts by electrospray ionization Fourier transform ion cyclotron resonance mass spectrometry. Energy Fuels 2004;18:1424–8.

[6] Barrow MP, McDonnel LA, Feng X, Walker J, Derrick PJ. The continued battle against corrosion. Anal Chem 2003;75:860–6.

[7] Vaz BG, Abdelnur PV, Rocha WFC, Gomes AO, Pereira RCL. Predictive petroleomics: measurement of the total acid number by electrospray Fourier transform mass spectrometry and chemometric analysis. Energy Fuels 2013;27:1873–80.

[8] Hemmingsen PV, Kim S, Pettersen HE, Rodgers RP, Sjoblom J, Marshall AG. Structural characterization and interfacial behavior of acidic compounds extracted from a north sea oil. Energy Fuels 2006;20:1980–7.

[9] Kim Y, Kim S. Improved abundance sensitivity of molecular ions in positive-ion APCI MS analysis of petroleum in toluene. J Am Soc Mass Spectrom 2010;21(3):386–92.

[10] Hur M, Yeo I, Park E, Kim YH, Yoo J, Kim E, et al. Combination of statistical methods and Fourier transform ion cyclotron resonance mass spectrometry for more comprehensive, molecular-level interpretations of petroleum samples. Anal Chem 2010;82:211–8.

[11] Teräväinem MJ, Pakarinem JMH, Wickström K, Vainiotalo P. Comparison of the composition of Russian and north sea crude oils and their eight distillation fractions studied by negative-ion electrospray ionization Fourier transform ion cyclotron resonance mass spectrometry: the effect of suppression. Energy Fuels 2007;21:266–73.

[12] Furimsky E, Massoth FE. Hydrodenitrogenation of petroleum. Catal Rev Sci Eng 2005;47(3):297–489.

[13] Van Looij F, Van der Laan P, Stork WHJ, DiCamillo DJ. Key parameters in deep hydrodesulfurization of diesel fuel. J Appl Catal A – Gen 1998;170(1):1–12.

[14] Wu Z, Rodgers RP, Marshall AG. Comparative compositional analysis of untreated and hydrotreated oil by electrospray ionization Fourier transform ion cyclotron resonance mass spectrometry. Energy Fuels 2005;19:1072–7.

[15] Hsu CS, Hendrickson CL, Rodgers RP, McKenna AM, Marshall AG. Petroleomics: advanced molecular probe for petroleum heavy ends. J Mass Spectrom 2011;46:337–43.

[16] Gaspar A, Schrader W. Expanding the data depth for the analysis of complex crude oil samples by Fourier transform ion cyclotron resonance mass spectrometry using the spectral stitching method. Rapid Commun Mass Spectrom 2012;26:1047–52.

[17] Benassi M, Arton B, Romão W, Babayev E, Rompp A, Spengler B. Petroleum crude oil analysis using low-temperature plasma mass spectrometry. Rapid Commun Mass Spectrom 2013;27:825–34.

[18] McKenna AM, Purcell JM, Rodgers RP, Marshall AG. Heavy petroleum composition. 1. Exhaustive compositional analysis of athabasca bitumen HVGO distillates by Fourier transform ion cyclotron resonance mass spectrometry: a definitive test of the Boduszynski model. Energy Fuels 2010;24:2929–38.

[19] Klein GC, Angstrom A, Rodgers RP, Marshall AG. Use of saturates/aromatics/resins/asphaultenes (SARA) fractionation to determine matrix effects in crude oil analysis by electrospray ionization fourier transform ion cyclotron resonance mass spectrometry. Energy Fuels 2006;20:668–72.

[20] Purcell JM, Merdrignac I, Rodgers RP, Marshall AG, Gauthier T, Guibard I. Stepwise structural characterization of asphaltenes during deep hydroconversion processes determined by atmospheric pressure photoionization (APPI) Fourier transform ion cyclotron resonance (FT-ICR) mass spectrometry. Energy Fuels 2010;24:2257–65.

[21] ASTM D5002-99 Standard Test Method for density; 2010.

[22] ASTM D1298-99 Standard Test Method for API degree; 2005.

[23] ASTM D664-09 Standard test Method for Acid Number of Petroleum Products by Potentiometric Titration.

[24] ASTM D7042–04 Standard Test Method for Dynamic Viscosity and Density of Liquids by Stabinger Viscometer (and the calculation of kinematic viscosity); 2004.

[25] ASTM D4294–10 Standard Test Method for Sulfur in Petroleum and Petroleum Products by Energy Dispersive X-ray Fluorescence Spectrometry; 2000.

[26] ASTM D 2892. Standard Test Method for Distillation of Crude Oil; 2005.

[27] Liu P, Shi Q, Chung KH, Zhang Y, Pan N, Zhao S, et al. Molecular characterization of sulfur compounds in Venezuela crude oil and its SARA fractions by electrospray ionization Fourier transform ion cyclotron resonance mass spectrometry. Energy Fuels 2010;24(9):5089–96.
[28] Liu P, Shi Q, Pan N, Zhang Y, Chung KH, Zhao S, et al. Distribution of sulfides and thiophenic compounds in VGO subfractions: characterized by positive-ion electrospray Fourier transform ion cyclotron resonance mass spectrometry. Energy Fuels 2011;25:3014–20.
[29] Colati KAP, Dalmaschio GP, de Castro EVR, Gomes AO, Vaz BG, Romão W. Monitoring the liquid/liquid extraction of naphthenic acids in brazilian crude oil using electrospray ionization FT-ICR mass spectrometry (ESI FT-ICR MS). Fuel 2013;108:647–55.
[30] Freitas S, Malacarne MM, Romão W, Dalmaschio GP, Castro EVR, Celante VG, et al. Analysis of the heavy oil distillation cuts corrosion by electrospray ionization FT-ICR mass spectrometry, electrochemical impedance spectroscopy, and scanning electron microscopy. Fuel 2013;104:656–63.
[31] Ding L, Rahimi P, Hawkins R, Bhatt S, Shi Y. Naphthenic acid removal from heavy oils on alkaline earth-metal oxides and ZnO catalysts. Appl Catal A – Gen 2009;371:121–30.
[32] Zhang A, Ma Q, Wang K, Liu X, Shuler P, Tang Y. Naphthenic acid removal from crude oil through catalytic decarboxylation on magnesium oxide. Appl Catal A – Gen 2006;303:103–9.
[33] Ferreira FN, Carneiro MC, Vaitsman DS, Pontes FVM, Monteiro MIC, da Silva LID, et al. Matrix-elimination with steam distillation for determination of short-chain fatty acids in hypersaline waters from pre-salt layer by ion-exclusion chromatography. J Chromatogr A 2012;1223:79–83.
[34] Stanford LA, Kim S, Rodgers RP, Marshall AG. Characterization of compositional changes in vacuum gas oil distillation cuts by electrospray ionization Fourier transform–ion cyclotron resonance (FT–ICR) mass spectrometry. Energy Fuels 2006;20:1664–73.
[35] Hughey CA, Hendrickson CL, Rodgers RP, Marshall AG. Kendrick mass defect spectroscopy: a compact visual analysis for ultrahigh-resolution broadband mass spectra. Anal Chem 2001;73:4676–81.
[36] Van Krevelen DW. Graphical-statistical method for the study of structure and reaction processes of coal. Fuel 1950;29:269–84.
[37] Huanga BS, Yinb WF, Sang DH, Jianga ZY. Synergy effect of naphthenic acid corrosion and sulfur corrosion in crude oil distillation unit. Appl Surf Sci 2012;259:664–70.
[38] Piehl RL. Naphthenic acid corrosion in crude distillation units. Mater Perform 1988;27:37–43.
[39] Slavcheva E, Shone B, Turnbull A. Review of naphthenic acid corrosion in oil refining. Br Corr J 1999;34:125–31.
[40] Alvisi PP, Lins VFC. An overview of naphthenic acid corrosion in a vacuum distillation plant. Eng Fail Anal 2011;18:1403–6.
[41] Smith DF, Rodgers RP, Rahimi P, Teclemariam A, Marshall AG. Effect of thermal treatment on acidic organic species from athabasca bitumen heavy vacuum gas oil, analyzed by negative-ion electrospray fourier transform ion cyclotron resonance (FT-ICR) mass spectrometry. Energy Fuels 2009;23:314–9.
[42] Mandal PC, Wahyudiono, Sasaki M, Goto M. Reduction of total acid number (TAN) of naphthenic acid (NA) using supercritical water for reducing corrosion problems of oil refineries. Fuel 2012;94:620–3.
[43] Shi Q, Zhao S, Xu Z, Chung KH, Zhang Y, Xu C. Distribution of acids and neutral nitrogen compounds in a Chinese crude oil and its fractions: characterized by negative-ion electrospray ionization fourier transform ion cyclotron resonance mass spectrometry. Energy Fuels 2010;24:4005–11.